Manuscript version: Author's Accepted Manuscript

The version presented in WRAP is the author's accepted manuscript and may differ from the published version or Version of Record.

Persistent WRAP URL:

http://wrap.warwick.ac.uk/108516

How to cite:

Please refer to published version for the most recent bibliographic citation information.
If a published version is known of, the repository item page linked to above, will contain details on accessing it.

Copyright and reuse:

The Warwick Research Archive Portal (WRAP) makes this work by researchers of the University of Warwick available open access under the following conditions.

Publisher's statement:

Please refer to the repository item page, publisher's statement section, for further information.

For more information, please contact the WRAP Team at: wrap@warwick.ac.uk.

warwick.ac.uk/lib-publications

1   **Simultaneous Stabilization of Pb and Improvement of Soil Strength using nZVI**

2   **Abstract**

3   This study demonstrates the feasibility of nanoscale Zero-Valent Iron (nZVI) for simultaneous

4   stabilization of Pb and improvement of soil strength via batch experiments. The soil samples

5   were prepared using slurry and pre-consolidation method at nZVI doses of 0.2%, 1%, 5%, and

6   10% (by dry weight). The physicochemical and geotechnical properties of Pb-contaminated

7   soil treated by nZVI were analyzed. The results indicate that the contamination of Pb(II)

8   resulted in a notable reduction in the undrained shear strength of soil from 16.85 kPa to 7.25

9   kPa. As expected, the Pb in exchangeable and carbonate-bound fractions decreased

10   significantly with the increasing doses of nZVI. Meanwhile, the undrained shear strength of

11   Pb-contaminated soil enhanced substantially as the increase of nZVI, from 25.83 kPa (0.2%

12   nZVI treatment) to 69.33 kPa (10% nZVI treatment). An abundance of bubbles, generated from

13   the oxidation of nZVI, was recorded. The mechanisms for simultaneous stabilization of Pb and

14   soil improvement primarily include: 1) the precipitation and transformation of Pb-/Fe- hydrated

15   oxides on the soil particles and their induced bounding effects; 2) the increased drainage

16   capability of soil as the occupation of nZVI aggregates and bubbles in the macropores space

17   and 3) the lower soil density derived from the increase in microbubbles retained in the soil.

18   This study is provided to facilitate the application of nZVI in the redevelopment of

19   contaminated soil.

20

21   **Keywords:** nZVI; lead, contaminated soil; physicochemical property; undrained shear strength

22

1 Introduction

Nanoscale Zero-Valent Iron (nZVI) is a well-established nanoparticle that has been used widely in the remediation of contaminated soil and groundwater (Bartke et al., 2018). The purpose of using nZVI is to remove or to stabilize the pollutants so that to reduce the potential threats caused by the pollutants to the ecology (Chen et al., 2017). Considerable endeavors have been made to improve the efficiency of NZVI in field appplication, such as degradation of various pollutants, mobility in subsurface, and revealing the fate and impacts of NZVI on ecology (Huang et al., 2016; Vilardi et al., 2018).

Nevertheless, civil engineers consider both the pollutants and the injected nZVI as non-native components of soil. Their concerns stem mainly from the geotechnical properties of remedied contaminated soil because these properties are important in the follow-up construction on the contaminated site or the reuse of contaminated soil, such as backfill at another site. The introduction of nZVI and its derived removal of contaminants in soil could potentially disturb the micro-structures of soil and lead to alteration of its geotechnical properties. This means that the application of nZVI in remediation of contaminated site may pose potential threat to serviceability, and reliability of a facility. Just like the ecological and human health risk posed by contamination, the geoenvironmental risk may break out at some point in the future, considering the high reactivity of nZVI and its long-term effect on the physicochemical properties of soil (Clayton, 2001). Thus, it is significant to investigate the behavior and mechanism of nZVI treatment in changing of geotechnical properties of soil. However, few studies have thoroughly addressed the effects of nZVI in this regard.

Most authorities accept that chemical contaminants are capable of changing properties of soil, either by directly changing the chemical or physical state of the soil, or through indirect changes, such as influencing biological activity and groundwater, which in return, modifies its properties (Ma et al., 2018; Xu et al., 2018). Rogers et al. (2004) found that the contamination of Pb^{2+} and Fe^{3+} had a significant effect on the initiation and development of the lime-clay reactions during both short-term modification and longer-term solidification. Dror et al. (2015) summarized that engineered nanomaterials have the potential to inflict irreversible changes on the physical and

chemical properties of pristine soils. Gil-Diaz et al. (2014) concluded that an immobilization of Pb^{2+} and Zn^{2+} by nZVI posed no negative effects for physicochemical and biological properties of soil. However, their researches did not reveal the changes in its geotechnical properties associated with their physicochemical counterpart, such as the shear strength of the soil which is the most important parameter in the design of civil engineering projects, neither did it reveal the mechanism of the effects. The reader should note that the changes in physicochemical and biological properties of soil do not always result in significant changes in the its geotechnical properties. For instance, Cuisinier et al. (2011) reported that no evidence showed any impact of chloride on the geotechnical behavior of their tested soils. Nasehi et al. (2016) performed an investigation of the effects of nZVI and nanoscale hydrated lime on the geotechnical characteristics of a diesel-contaminated soil. They suggested that the introduction of nZVI to the diesel-contaminated soil led to an increase in Unconfined Compressive Strength (UCS), maximum dry density, optimum water content, and shear strength parameters. Nevertheless, the mechanism of nZVI in soil improvement remains ambiguous given that oxidation, adsorption, and precipitation may be involved in the removal of diverse contaminants.

This study is an investigation of the stabilization of lead by nZVI in a clayey soil and its effects on the geotechnical properties of soil. Particularly, lead (Pb), a heavy metal of well-known toxicity, prevalence and responsible for liver and kidney damage, anemia, infertility, and mental retardation among other consequences, is employed as an artificial contaminant (Huang et al., 2018). Different doses of nZVI were added to the Pb-contaminated soil. The mobilization effect on lead ions, physicochemical characterization, and shear strength of the soil were examined to analyze the effects of nZVI on the physicochemical and geotechnical properties of the Pb-contaminated earth. The results of this study can facilitate the application of nZVI in the remediation of contaminated sites where remedied soil will be used as backfill, such as remediation of brownfield and dredged sediment.

2 Methodology

2.1 Soil Preparation

The researcher collected the soil samples from a construction site in Areia Preta, Macau (N22°12'35.84", E113°33'27.96"). According to the Unified Soil Classification System (USCS, ASTM D2487-17), the Atterberg limits of the preconcerted soil were found to be 61, 32, and 29 for the liquid limit, plastic limit, and plasticity index respectively. The particle size distribution, when analyzed by the Malvern Particle Size Analyzer indicated that the D60, D30, and D10 values were 8.5, 3.08, and 1.01 mm respectively. The soil was classified as MH: silt with high plasticity.

The slurry and pre-consolidation method was employed to prepare the soil samples (Choudhary et al., 2016). Firstly, the soil was first cut into small chunks and immersed in distilled water for two days, after which the soil fractions were passed through a No. 16 sieve (1 mm opening) to achieve a soil slurry. The water content of the obtained slurry was increased up to twice of the liquid limit with vivid agitation for approximately 10 minutes to obtain a homogeneous state. Subsequently the slurry (approximately 17 kg for each) was subjected to pre-consolidation in a container under an overburden pressure of 200 kPa (Indraratna and Redana, 1998). When the settlement of pre-consolidation was stable (usually took two weeks), soil samples with a height of 84 mm and diameter of 38 mm were trimmed.

For the preparation of Pb-contaminated soil, artificial pollutant of lead nitrate ($Pb(NO_3)_2$) (AR, powder solid state) at the lead mass ratio of 400 mg/kg (dry soil mass) was added to the soil slurry (the weight of the soil slurry was approximately 120 kg). To achieve a homogeneous state, the spiked soil slurry was mechanically stirred for approximately 10 mins. Then, the spiked slurry was matured for two weeks to achieve equilibrium of adsorption and desorption prior to pre-consolidation or further treatment. As for the preparation of nZVI treated soil samples, 0.2%, 1%, 5%, and 10% (mass ratio of nZVI to the spiked dry soil) nZVI were added respectively to the aged Pb-spiked soil slurry and agitated vividly prior to pre-consolidation. The nZVI was supplied by Shanghai Xiangtian Nano Materials Co., LTD. The average diameter of nZVI used in this study was about 50 nm, with a specific area of 30 m^2/g (provided by the manufacturer).

Figure 1 summarizes the experimental procedure. For all the natural, Pb-contaminated and nZVI treated soil samples, sequential extraction procedure, shear strength tests, and characterization were carried out to investigate the mechanism of the effect of nZVI treatment on the physicochemical and geotechnical properties of the treated clayey soil.

2.3 Shear Strength of Soil

The Laboratory Vane Shear Test (Wykeham Farrance, 27-WF1730) was conducted to evaluate the undrained shear strength of the soil samples, as per the Standard Test Method for Laboratory Miniature Vane Shear Test for Saturated Fine-Grained Clayey Soil (American Society for Testing Material, ASTM D4648/D4648M-13). Particularly, two kinds of vane blade with the same width of 12.7 mm, yet the different heights of 19 mm and 12.7 mm were employed. The rotation rate of the vane during testing was maintained at approximately 6°/min.

2.4 Characterization and Testing

The mineralogy of the soil was characterized by X-ray diffraction (XRD) on Rigaku Smartlab (anode Cu, in configuration θ/2θ, with an acceleration tension of 45 kV and a current of 200 mA), at a scanning rate of 2.0 °/min. Prior to the XRD test, the soil samples were smashed and crushed into soil chip with a thickness of approximately 0.5 mm after freeze drying for 24 h. The pore structure characteristics of the soil were quantitatively described by Mercury Intrusion Porosimetry (MIP) using a Mercury Porosimeter AutoPore IV 9510 (Micromeritics Instruments Co., USA). Before the MIP measurements, the soil samples were dried using the vacuum freeze-drying method for 24 hours. Washburn's equation was involved to calculate the relationship between the mercury pressure and pore structure characteristics (Abell et al., 1999). The soil particle size distribution was characterized by a laser particle size analyzer (Malvern, Mastersizer 3000) in distilled water solution, assisted by the continuous ultrasound dispersion (40W, 40kHz) and electric mixing (3000 rpm).

The availability of Pb in soil samples was analyzed after applying the Modified Sequential Extraction Procedure proposed by Tessier et al. (1979) using Inductively Coupled Plasma Mass Spectrometry (ICP-MS, Agilent 7700X). Soil pH was measured according to the International Standard Soil Quality-Determination of pH (ISO 10390: 2005). The total carbon (TC) of soil

samples was analyzed by Analytik Jena (Multi N/C 3100 and 1300) after undergoing air drying at 35 °C for 12 hours. Zeta potential and electrical conductivity of soil samples were collected by a zeta potential analyzer using phase analysis light scattering (Brookhaven ZetaPALS) at a soil concentration of 1g/L in distilled water.

**3 Results and Discussion**

3.1 Phenomenon and Theory

Changes of physicochemical and geotechnical properties of soil are invariably associated with the microscopic change of the soil body. In this study, the specific behavior occurred during the preparation of the soil sample which was recorded to examine the effect of nZVI on the geotechnical properties of soil.

In this study, a mass of bubbles with a size of a few micrometers was observed in the soil slurry after nZVI treatment (before pre-consolidation), as shown in Figure 2. Accordingly, a copious quantity of microbubble prints remained in the soil sample following said process, as shown in Figure 2 (c). For all nZVI-treated soil samples, the phenomena of nZVI aggregations was detected in the wake of acute agitation of the soil slurry and nZVI. The appearance of micro-bubbles and fissures intensified when the dose of nZVI was increased.

This specific phenomenon provides unequivocal evidence of the interaction between nZVI and the clay slurry. In fact, this is reasonable because the nanosized Fe^0 exhibited a markedly increased extent of corrosion under both the anaerobic and aerobic conditions (Reardon, 1995; Reardon et al., 2008). In an aerobic condition, nZVI is easily oxidized to ferrous iron, with protons being consumed in the process (Li et al., 2006):
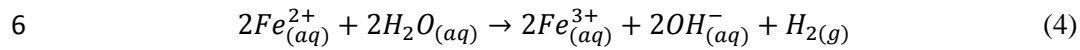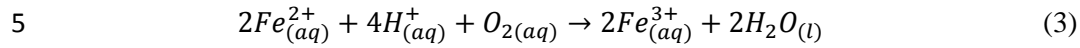
$$2Fe^0_{(s)} + 4H^+_{(aq)} + O_{2(aq)} \rightarrow 2Fe^{2+}_{(aq)} + 2H_2O_{(l)} \tag{1}$$
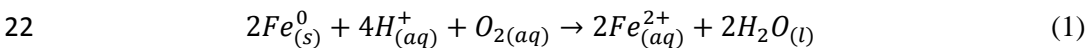
When oxygen is exhausted or in the absence of oxygen, fresh nZVI tends to experience a rapid oxidation phase upon entering the aqueous phase:

$$Fe^0_{(s)} + 2H_2O_{(aq)} \rightarrow Fe^{2+}_{(aq)} + 2OH \cdot_{aq} + H_{2(g)} \tag{2}$$
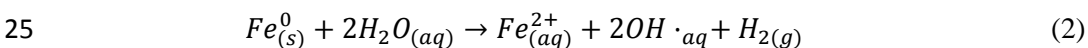
In this reaction (2), two molecules of water are consumed for every mole of iron corroded. Meanthile, one molecule of hydrogen gas and two molecules of hydroxy radicals are generated.

In addition to the ferrous ions and hydrogen gas, hydroxyl ions are also generated which will increase the media pH, while hydrogen ions are consumed. Moreover, if oxygen is sufficient in the slurry, ferrous ions will undergo further oxidative transformation to become ferric ions until the oxygen is exhausted (Lefevre et al., 2016):

$$2Fe^{2+}_{(aq)} + 4H^+_{(aq)} + O_{2(aq)} \rightarrow 2Fe^{3+}_{(aq)} + 2H_2O_{(l)} \tag{3}$$

$$2Fe^{2+}_{(aq)} + 2H_2O_{(aq)} \rightarrow 2Fe^{3+}_{(aq)} + 2OH^-_{(aq)} + H_{2(g)} \tag{4}$$

Continued corrosion of iron and generation hydroxyl ions lead to saturation and precipitation of Fe(OH)$_2$ on the soil particles in the slurry, itself a relatively insoluble solid phase. In the absence of oxygen (or anoxic conditions) and at low temperatures, Fe(OH)$_2$, is controlled by the pH value of the system but is predicted thermodynamically to convert to magnetite or other iron minerals (Liu et al., 2015):

$$3Fe(OH)_{2(s)} \rightarrow Fe_3O_{4(s)} + 2H_2O_{(l)} + H_{2(g)} \tag{5}$$
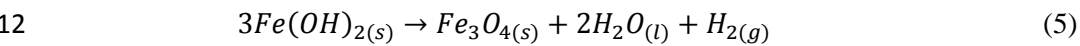
Based on the previously stated theoretical foundation, the speculated is that iron minerals are formed from ferrous and ferric ions in the aqueous phase of the soil slurry and may precipitate on the soil particles and subsequently bond them together, with nZVI aggregates centralized. Clearly, these micro-bubbles are generated primarily from the oxidation of nZVI in the aqueous phase and are retained in the soil sample. In addition to that, the nitrogen and carbon dioxide, generated by the reduction of nitrate by nZVI and oxidation of natural organic matters in soil, respectively, may also contribute partially to the generation of micro-bubbles (Vilardi and Di Palma, 2017; Vilardi et al., 2017, 2018). The increased the drying shrinkage occurred due to the reduced water content lead to the occurrence of massive fissures grown on the surface of nZVI-treated soil slurry.

3.2 Microstructure

A laser particle size analyzer was used to quantify the physical changes of soil particle size, as demonstrated in Figure 3. In all cases, the soil particles stuck together in anomalous clumps after undergoing pre-consolidation in the container, with the particle sizes varying from 400 nm to 1 mm. No distinct nZVI particle was observed in the soil particles. The decomposition

of soil particles by lead nitrate led to an increase in clay and silt clay fractions, which reduced the average size of soil particles. Analogously, the introduction of nZVI resulted in a significant decrease in the size of nZVI treated soil particles. The particle size gravitated toward a decreasing value with increasingly large doses of nZVI. The thinking is that the oxidation and the subsequent growth of iron particles from the nano-level to micron level instigated the reduction in particle size. For the 10% nZVI-treated soil sample, the sand fraction in the soil went up to 16%. Such increase can be ascribed to the prevailing of the increased pozzolanic-like reaction of the nZVI-induced iron minerals' precipitation among the soil particles (Nasehi et al., 2016).

As already noted, a mass of microbubbles and residual bubble prints were observed. They were generated primarily from the oxidation of nZVI in the aqueous phase, as well as the reduction of nitrate. Actually, for the remediation of the contaminated site by the injection of chemical remediation materials, bubbles are the common coproducts during the mineralization of contaminants, such as those involved in In-situ Chemical Oxidation (ISCO) using hydrogen peroxide (H_2O_2), Micro-Nano Bubbles (MNBs) and persulfate (Liu et al., 2014). Soil pore characteristics, including the total volume, size distribution, and shape of soil pore spaces are important indicators that determine workability and friability of soil (Munkholm et al., 2016; Obour et al., 2017). However, little is known about the link between remediation-derived soil pore characteristics, and physicochemical and geotechnical properties of soil.

To improve the understanding of bubbles and their effect on the geotechnical properties of soil, its pore structure characteristics were quantitatively described by MIP, as shown in Figure 4 and Table 1. The results indicate that the pore size diameter of all soil samples mainly ranged from 10 nm to 10 um, which can be classified as mesopore (2-50 nm) and macropore (> 50 nm) (Anovitz and Cole, 2015). The introduction of lead nitrate resulted in an evident increase of average pore diameter, which is in accordance with its appearance (as shown in Figure 2a). When the amount of added nZVI was 0.2% in the mass ratio of dry soil (Pb-contaminated soil), the average pore diameter mushroomed from 90.4 nm to 178.4 nm. Accordingly, a sharp drop in the total pore area was recorded. With the increase in added nZVI, the average pore diameter

decreased, with a corresponding increase in total pore area. Furthermore, the increase in nZVI was met with a reduction in the amount of macropores (>50 nm) and a rise in mesopores (2-50 nm). The 10% nZVI-treated soil samples held the highest total pore area. On the other hand, along with the decrease in the amount of macropores and the increase in mesopores, both the density and porosity of nZVI-treated soil samples gradually increased. However, the 0.2% nZVI treated soil samples presented the lowest values of density and porosity among all the samples, while the10% nZVI treated soil sample showed a tiny drop in the values of density and porosity. The speculated theory is that a dynamic equilibrium exists between the decrease in macropores space caused by the occupation of nZVI aggregates and the increase in microbubbles retained in the saturated soil (Soares et al., 2018).

3.3 X-ray Diffraction (XRD)

The X-ray diffraction (XRD) patterns of the soil samples are displayed in Figure 5. The selected soil was composed primarily of quartz (PDF#85-1054, ICSD Minerals), laumontite $Ca_4(Al_8Si_{16}O_{48}(H_2O)_{18}$ (PDF#80-0150, ICSD Minerals), and greenalite $Fe_6Si_4O_{10}(H_2O)_{18}$ (PDF#72-0177, ICSD Minerals). The main characteristic peaks revealed a slight discordance among the soil samples, implying that distortion occurred in the lattice of minerals after the introduction of nZVI. The assumption is that the frameworks of certain mineral crystals were doped by Fe(Ⅱ), Fe(Ⅲ), and Pb(Ⅱ) of larger atomic radius, resulting in the appreciable changes in lattice parameters (Castaldi et al., 2008), as shown in Table 2. Lattice parameters of laumontite mineral in the soil samples altered irregularly with the introduction of lead nitrate as well as the nZVI. A minute difference in weak characteristic peaks can be perceived at 2-Theta of 17.8°, 27.6°, 35.7°, and 36.6°, which can be credited to the iron mineral crystals of magnetite Fe_3O_4 (PDF#89-0950), ferrosilite $FeSiO_3$ (PDF#76-0887, ICSD Minerals), hematite Fe_2O_3 (PDF#85-0987, ICSD Minerals), and goethite $FeOOH$ (PDF#81-0464) respectively (Huang et al., 2013). The presence of deuterogenic and different iron minerals will constitute the highly-disordered multilayer of amorphous core shell construction on the surface of nZVI and soil particles with a thickness of approximately several nanometers (Arancibia-Miranda et al., 2014).

9

For the nZVI in the oxidation system, on the one hand, the reduction of Pb^{2+} will be suppressed because of isolation resulting from the multilayer core shell construction (Xue et al., 2018). On the other hand, the corrosion byproducts can greatly promote the co-precipitation and adsorption of Pb^{2+} and improve the stabilization capability of nZVI. However, the characteristic peaks associated with reduced lead and related lead oxides were not clearly presented in the diffractogram of nZVI-treated soil samples, which may have been a consequence of 1) the Pb being of a trace amount in the soil, as well as 2) the crystalline structures of reduced lead and related lead oxides being amorphous.

3.4 Metal Immobilization

Because heavy metals do not undergo microbial or chemical degradation, the total concentration of these metals persists for a long time after their introduction in soils. The ecological toxicities of heavy metals in soil are primarily controlled by their available fraction because they are readily mobile and bioavailable within the environment and can potentially be taken up by plant roots to enter the food chain (Hou et al., 2013; Roy and Mcdonald, 2015). In this sense, the immobilization of heavy metals in soil offers a promising strategy for achieving the redistribution of contaminants from the solution phase to more geochemically stable phases, thereby reducing their bioavailability and transportation in the environment (Bolan et al., 2014). Many studies have demonstrated the excellent immobilization capacity of nZVI for various heavy metal ions, in both soil and groundwater (Gil-Díaz et al., 2017). The widely accepted thinking is that the mechanism of nZVI for immobilization of Pb in an aqueous system is controlled by a sorption process, reduction of Pb^{2+} to Pb^{0}, and (co)precipitation (Wang et al., 2016; Gil-Diaz et al., 2017).

In this study, the effects of nZVI on the immobilization of Pb in soil samples were examined by comparing the distribution of lead in different soil fractions. Figure 6 displays the concentration distribution tendency of the quantity of lead retained in the soil samples. With the introduction of lead nitrate, the lead in the exchangeable (EX), carbonate-bound (CB), organic matter-bound (OM), and the residual (RS) fractions increased significantly, compared with that in the natural soil. As expected, the lead in the more easily available fractions, namely

1 EX and CB, was evidently decreased by the introduction of nZVI. Then increasing in the nZVI

2 amount, a diminishing concentration in the EX, CB, and OM fractions was observed. These

3 more easily available fractions have higher leachability and bioaccessibility than others

4 (Alloway, 2013; Zong et al., 2016). Thus, the application of nZVI can effectively immobilize

5 the lead in soil and lower the risk to humans and environmental organisms. By contrast, the

6 lead in Fe/Mn oxides-bound and residual fractions increased when nZVI added. This was

7 reasonable because of the increase in irons, and part of Fe/Mn oxides-bounded lead converted

8 to a more strongly bound complex. Moreover, part of this decomposition of organics, resulting

9 from the introduction of nZVI, may lead to a descending concentration of lead in the organic-

10 bound fraction, as shown in Table 1, and subsequently, an increased lead concentration in other

11 fractions. In all cases, most of the volume of lead was bound by organic matter and Fe/Mn

12 oxides, followed by a residual fraction, exchangeable fraction, and carbonate-bound fractions.

13 **3.5 Undrained Shear Strength**

14 To reveal the variations and features of geotechnical properties of soil, as a consequence of

15 contamination and remediation, was the main objective of this study. In the interests of

16 evaluating the effects of nZVI on the geotechnical properties of soil, undrained vane shear

17 strength (S_u) was investigated. The shear strength of a soil is defined as the maximum shear

18 stress that it can sustain under loading (Türkel, 2007). According to Stavi et al. (2016), the

19 moisture content of a soil is a crucial parameter in controlling the shear strength of clays. Figure

20 7 shows the results of vane shear strength together with the corresponding moisture content.

21 The results indicate that the S_u of natural soil dropped sharply after the introduction of lead

22 nitrate, from 16.82 kPa to 7.25 kPa. Correspondingly, the moisture content increased from

23 50.78% to 56.89%. Meanwhile, the zeta potential of soil dropped analogously from -16.14 mV

24 to -6.31 mV (Table 1), pointing to a notable decrease in soil stability. This phenomenon may

25 be another signal that explains the obvious decrease of S_u.

26 On a positive note, the S_u of Pb-contaminated soil was improved remarkably when treated

27 with nZVI. Figure 6 shows us that even the 0.2% amount of nZVI can strengthen the soils'

28 undrained shear strength from 7.25 kPa to 25.38 kPa. The S_u of soil was increased with the rise

1   in nZVI, but the acceleration rate decreased when the mass ratio of nZVI to dry soil was 10%.

2   Correspondingly, the moisture content of soil exhibited a negative trend to the S_u when the dose

3   of nZVI treatment was increased from 0.2% to 5%. That is, the soil moisture content decreased

4   with the increasing doses of nZVI. This can be presumably ascribed to the padding of nZVI

5   and its volume expansion by oxidation in the soil pore, which resulted in an extrusion of the

6   water. However, an unexpected situation for the 10% nZVI-treated soil was that a soaring of

7   its moisture content to 55.77%, along with further enhancement of the S_u of the soil sample up

8   to 69.33 kPa, was recorded. This can be put down to being a consequence of the changes in

9   both soil constituent and structure. On the one hand, the addition of 10% nZVI is at a high

10   percentage load with the forceful capacity of oxidation reaction to change the soil constituent

11   (Gil-Diaz et al., 2014); the increased water holding capacity can be partially attributed to the

12   generation of iron oxide-hydroxides such as ferrihydrite ($Fe_5HO_8 \cdot 4H_2O$), schwertmannite

13   ($Fe_8O_8(OH)_6(SO) \cdot nH_2O$), and goethite ($\alpha$-FeOOH) (Velimirovic et al., 2018; Zhang et al.,

14   2016). On the other, an increase in microbubbles enabled itself to readily adsorb moisture and

15   humidity (Lawrence and Jiang, 2017). Luxurious nZVI may give rise to a hardened soil, making

16   it difficult to drain under the consolidation pressure of 200 kPa and thus contributing to an

17   exceptionally high moisture retaining capacity (Burgess et al., 2016). Furthermore, with regard

18   to the microbubbles and their bubble prints in the soil samples, the presumption was that these

19   micron-level bubble-prints were the residual channeled network of voids for the drainage

20   boundary (Acharya et al., 2015). However, the density and porosity of nZVI-treated soil

21   decreased synchronously. The changes of the soil components by nZVI treatment can be

22   responsible for this abnormal condition. As a rule, low density of a soil is usually associated

23   with low strength (Lawrence and Jiang, 2017). Because of the consuming oxidation of nZVI in

24   the soil, the Pb-contaminated soil turned out to be lightened and firmed.

25   Based on these above discussions, the conclusion can be drawn that the application of nZVI

26   can simultaneously stabilize Pb and improve the soil strength in the short-term, as a result of

27   which it can lower the risks involved in geotechnical engineering (Griffiths et al., 2012). The

28   Pb-contaminated soil became light, dense, and reinforced after nZVI treatment. The increase in

undrained shear strength can be primarily assigned to the precipitation and transformation of nZVI-induced iron minerals on the soil particles and their bonding together.

4 Conclusion

The application of nZVI in treating subsurface contaminants should be considered carefully because their intrusion may lead to the changes of geotechnical properties of soil, ultimately inducing potential geoenvironmental risks. In this study, the author investigated the effects of nZVI on the immobilization of lead and the undrained shear strength of soil. The results indicate that the introduction of Pb(II) in the natural soil resulted in a visible reduction in shear strength from 16.85 kPa to 7.25 kPa.

On a positive note, with the increasing doses of nZVI from 0.2% to10% (dry weight), the shear strength of lead-contaminated soil substantially increased from 25.83 kPa to 69.33 kPa. Moreover, increased dose of nZVI generally lead to increases in particle size (larger than 0.063 mm), amount of mesopore (2-50 nm), and decreases in the amount of macropore (>50 nm), moisture content and Pb bound to exchangeable and carbonate fractions. The oxidation of nZVI in the soil slurry gave rise to abundant micro-fissures, and bubbles equally appeared in the soil slurry and were retained in the soil samples, leaving bubble prints. The mechanisms for simultaneous stabilization of Pb and soil improvement can be primarily ascribed to the precipitation and transformation of Pb-/Fe- hydrated oxides on the soil particles and their induced bounding effects. Moreover, the increased drainage capability of soil as the occupation of nZVI aggregates and bubbles retained in the soil also contributed to the soil improvement.

Although nZVI aggregations were evident in the soil slurry, the feasibility of nZVI for simultaneous stabilization of Pb and improvement of soil strength is here confirmed. With respect to the wide application of nZVI and the follow-up infrastructure construction on the contaminated site (such as brownfields), the results of this study can facilitate the remediation of metals-contaminated soil and recovery of contaminated soil for civil engineering. However, the long-term effect of nZVI treatment on the geotechnical properties of soil and structural stabilities should be revealed in future study.

Acknowledgements

Reference

Abell A. B., Willis K. L., Lange D. A., 1999. Mercury Intrusion Porosimetry and Image Analysis of Cement-Based Materials. Journal of Colloid & Interface Science. 211(1), 39-44. https://doi.org/10.1006/jcis.1998.5986.

Acharya M. P., Hendry M. T., Martin C. D., 2015. Effect of gas bubbles on pore pressure response in peat beneath a rail. Canadian Geotechnical Journal. 53(5), 765-772. https://doi.org/10.1139/cgj-2015-0122.

Alloway B. J., 2013. Sources of Heavy Metals and Metalloids in Soils. In: Alloway BJ, editor. Heavy Metals in Soils: Trace Metals and Metalloids in Soils and their Bioavailability. Springer Netherlands, Dordrecht. 11-50. https://doi.org/10.1007%2F978-94-007-4470-7_2.

Anovitz L. M., Cole D. R., 2015. Characterization and Analysis of Porosity and Pore Structures. Reviews in Mineralogy & Geochemistry. 80, 61-164. http://doi.org/10.2138/rmg.2015.80.04.

Arancibia-Miranda N., Baltazar S. E., Garcia A., Romero A. H., Rubio M. A., Altbir D., 2014. Lead removal by nano-scale zero valent iron: Surface analysis and pH effect. Materials Research Bulletin. 59, 341-348. http://doi.org/10.1016/j.materresbull.2014.07.045.

ASTM D4648/D4648M-16, 2016. Standard Test Methods for Laboratory Miniature Vane Shear Test for SaturatedFine-Grained Clayey Soil. ASTM International, West Conshohocken, PA. http://doi.org/10.1520/D4648_D4648M-16.

ASTM D2487-17, 2017. Standard Practice for Classification of Soils for Engineering Purposes (Unified Soil Classification System). ASTM International, West Conshohocken, PA. http://doi.org/10.1520/D2487-17.

Bartke S., Hagemann N., Harries N., Hauck J., Bardos P., 2018. Market potential of nanoremediation in Europe-Market drivers and interventions identified in a deliberative scenario approach. Science of The Total Environment. 619, 1040-1048. http://doi.org/10.1016/j.scitotenv.2017.11.215.

Bian R., Cheng K., Zheng J., Liu X., Liu Y., Li Z., et al., 2015. Does metal pollution matter with C retention by rice soil? Scientific reports. 5, 13233. http://doi.org/10.1038%2Fsrep13233.

Bolan N., Kunhikrishnan A., Thangarajan R., Kumpiene J., Park J., Makino T., et al., 2014. Remediation of heavy metal(loid)s contaminated soils – To mobilize or to immobilize? Journal of Hazardous Materials. 266, 141-166. https://doi.org/10.1016/j.jhazmat.2013.12.018.

Burgess D. T., Kettler R. M., Loope D. B., 2016. The Geologic Context of Wonderstone: A Complex, Outcrop-Scaled Pattern of Iron-Oxide Cement. Journal of Sedimentary Research. 86(5), 498-511. https://doi.org/10.2110/jsr.2016.35.

Castaldi P., Santona L., Enzo S,. Melis P., 2008. Sorption processes and XRD analysis of a natural zeolite exchanged with Pb^{2+}, Cd^{2+} and Zn^{2+} cations. Journal of Hazardous Materials. 156, 428-434. https://doi.org/10.1016/j.jhazmat.2007.12.040.

Chen A., Shang C., Shao J., Zhang J., Huang H., 2017. The application of iron-based technologies in uranium remediation: A review. Science of The Total Environment. 575, 1291-1306. https://doi.org/10.1016/j.scitotenv.2016.09.211.

Choudhary K., Indraratna B., Rujikiatkamjorn C., 2016. Pore pressure based method to quantify smear around a vertical drain. Géotechnique Letters 6(3), 1-5. https://doi.org/10.1680/jgele.16.00065.

Cuisinier O., Le Borgne T., Deneele D., Masrouri F., 2011. Quantification of the effects of nitrates, phosphates and chlorides on soil stabilization with lime and cement. Engineering Geology. 117, 229-235. https://doi.org/10.1016/j.enggeo.2010.11.002.

Clayton, C. R. I., 2001. Discussion: Managing geotechnical risk: time for change? Geotechnical Engineering. 155(1), 79-80. https://doi.org/10.1680/geng.2001.149.1.3.

Dror I., Yaron B., Berkowitz B., 2015. Abiotic soil changes induced by engineered nanomaterials: A critical review. Journal of Contaminant Hydrology. 181, 3-16. https://doi.org/10.1016/j.jconhyd.2015.04.004.

Fridriksson T., Bish David L., Bird Dennis K., 2003. Hydrogen-bonded water in laumontite I: X-ray powder diffraction study of water site occupancy and structural changes in laumontite during room-temperature isothermal hydration/dehydration. American Mineralogist. 88(2-3), 277–287. http://dx.doi.org/10.2138/am-2003-2-304.

Gil-Díaz M., Alonso J., Rodríguez-Valdés E., Gallego J. R., Lobo M. C., 2017. Comparing different commercial zero valent iron nanoparticles to immobilize As and Hg in brownfield soil. Science of The Total Environment; 584, 1324-1332. https://doi.org/10.1016/j.scitotenv.2017.02.011.

Gil-Diaz M. M., Perez-Sanz A., Vicente M. A., Lobo M. C., 2014. Immobilisation of Pb and Zn in Soils Using Stabilised Zero-valent Iron Nanoparticles: Effects on Soil Properties. Clean-Soil Air Water. 42, 1776-1784. https://doi.org/10.1002/clen.201300730.

Griffiths D. V., Huang J., Fenton G. A., 2012. Risk assessment in geotechnical engineering: Stability analysis of highly variable soils. Geotechnical Special Publication. 90(226), 78-101. https://doi.org/10.1061%2F9780784412138.0004.

Hou D., He J., Lü C., Ren L., Fan Q., Wang J., et al., 2013. Distribution characteristics and potential ecological risk assessment of heavy metals (Cu, Pb, Zn, Cd) in water and sediments from Lake Dalinouer, China. Ecotoxicology and Environmental Safety. 93, 135-144. https://doi.org/10.1016/j.ecoenv.2013.03.012.

Huang D., Qin X., Peng Z., Liu Y., Gong X., Zeng G., Huang C., Cheng M., Xue W., Wang X., Hu Z., 2018. Nanoscale zero-valent iron assisted phytoremediation of Pb in sediment: Impacts on metal accumulation and antioxidative system of Lolium perenne. Ecotoxicology and Environmental Safety. 153, 229-237. https://doi.org/10.1016/j.ecoenv.2018.01.060.

Huang D., Xue W., Zeng G., Wan J., Chen G., Huang C., Zhang C., Cheng M., Xu P., 2016. Immobilization of Cd in river sediments by sodium alginate modified nanoscale zero-valent iron:

Impact on enzyme activities and microbial community diversity. Water Research. 106, 15-25. https://doi.org/10.1016/j.watres.2016.09.050.

Huang P., Ye Z., Xie W., Chen Q., Li J., Xu Z. et al., 2013. Rapid magnetic removal of aqueous heavy metals and their relevant mechanisms using nanoscale zero valent iron (nZVI) particles. Water Research. 47, 4050-4058. https://doi.org/10.1016/j.watres.2013.01.054.

Indraratna B., Redana I. W., 1998. Laboratory determination of smear zone due to vertical drain installation. Journal of Geotechnical and Geoenvironmental Engineering. 124, 180-184. http://doi.org/10.1061/(ASCE)1090-0241(1998)124:2(180).

ISO 10390: 2005. Soil Quality—Determination of pH (ISO 10390: 2005). Available at: https://www.iso.org/standard/40879.html.

Lawrence M., Jiang Y., 2017. Porosity, Pore Size Distribution, Micro-structure. In: Amziane S., Collet F. (eds) Bio-aggregates Based Building Materials. 23. https://doi.org/10.1007%2F978-94-024-1031-0_2.

Lefevre E., Bossa N., Wiesner M. R., Gunsch C. K., 2016. A review of the environmental implications of in situ remediation by nanoscale zero valent iron (nZVI): Behavior, transport and impacts on microbial communities. Science of The Total Environment. 565, 889-901. https://doi.org/10.1016/j.scitotenv.2016.02.003.

Li X., Elliott D., Zhang W., 2006. Zero-valent iron nanoparticles for abatement of environmental pollutants: Materials and engineering aspects. Critical Reviews in Solid State and Materials Sciences. 31, 111-122. https://doi.org/10.1080/10408430601057611.

Liu A., Liu J., Zhang W., 2015. Transformation and composition evolution of nanoscale zero valent iron (nZVI) synthesized by borohydride reduction in static water. Chemosphere. 119, 1068-1074. https://doi.org/10.1016/j.chemosphere.2014.09.026.

Liu H., Bruton T. A., Doyle F. M., Sedlak D. L., 2014. In Situ Chemical Oxidation of Contaminated Groundwater by Persulfate: Decomposition by Fe(III)- and Mn(IV)-Containing Oxides and Aquifer Materials. Environmental Science & Technology. 48, 10330. https://doi.org/10.1021/es502056d.

Ma F., Wu B., Zhang Q., Cui D., Liu Q., Peng C., et al., 2017. An innovative method for the solidification/stabilization of PAHs-contaminated soil using sulfonated oil. Journal of Hazardous Materials. 344, 742-748. https://doi.org/10.1016/j.jhazmat.2017.11.015.

Munkholm L. J., Heck R. J., Deen B., Zidar T., 2016. Relationship between soil aggregate strength, shape and porosity for soils under different long-term management. Geoderma. 268, 52-59. https://doi.org/10.1016/j.geoderma.2016.01.005.

Nasehi S. A., Uromeihy A., Morsali A., Nikudel M. R., 2015. Use of nanoscale zero-valent iron to improve the shear strength parameters of gas oil contaminated clay. Geopersia; 5, 161-175. http://dx.doi.org/10.22059/jgeope.2015.56093.

Nasehi S. A., Uromeihy A., Nikudel M. R., Morsali A., 2016a. Use of nanoscale zero-valent iron and nanoscale hydrated lime to improve geotechnical properties of gas oil contaminated clay: a comparative study. Environmental Earth Sciences. 75, 1-20. https://doi.org/10.1007/s12665-016-5443-6.

Obour P. B., Lamandé M., Edwards G., Sørensen C. G., Munkholm L. J., 2017. Predicting soil workability and fragmentation in tillage: a review. Soil Use and Management. 33, 288-298. https://doi.org/10.1111/sum.12340.

Reardon E. J., 1995. Anaerobic Corrosion of Granular Iron-Measurement and Interpretation of Hydrogen Evolution Rates. Environmental Science & Technology. 29, 2936-2945. https://doi.org/10.1021/es00012a008.

Reardon E. J., Fagan R., Vogan J. L., Przepiora A., 2008. Anaerobic corrosion reaction kinetics of nanosized iron. Environmental Science & Technology. 42, 2420-2425. https://doi.org/10.1021/es0712120.

Rogers C. D. F., Boardman D. I., Glendinning S., 2004. The influences of iron (III) and lead (II) contaminants on lime-stabilised clay. Géotechnique. 54, 467-486. https://doi.org/10.1680/geot.2004.54.7.467.

Roy M., Mcdonald L. M., 2015. Metal Uptake in Plants and Health Risk Assessments in Metal-Contaminated Smelter Soils. Land Degradation & Development. 26, 785-792. https://doi.org/10.1002/ldr.2237.

Soares A., Ramos S., Albergaria T., Delerue-Matos C., 2018. Green zero valent iron nanoparticles dispersion through a sandy column using different injection sequences. Science of The Total Environment. 637, 935-942. https://doi.org/10.1016/j.scitotenv.2018.05.096.

Stamatelatou K., Antonopoulou G., Lyberatos G., Luque R., Campelo J., Clark J., 2011. Production of biogas via anaerobic digestion. Handbook of Biofuels Production (Second Edition). 259-301. https://doi.org/10.1016/B978-0-08-100455-5.00010-2.

Stavi I., Barkai D., Knoll Y. M., Zaady E., 2016. Livestock grazing impact on soil wettability and erosion risk in post-fire agricultural lands. Science of The Total Environment. 573, 1203-1208. https://doi.org/10.1016/j.scitotenv.2016.03.126.

Tessier A., Campbell P. G. C., Bisson M., 1979. Sequential Extraction Procedure for the Speciation of Particulate Trace-Metals. Analytical Chemistry. 51, 844-851. https://doi.org/10.1021/ac50043a017.

Türkel S., 2007. Strength properties of fly ash based controlled low strength materials. Journal of Hazardous Materials. 147, 1015-1019. https://doi.org/10.1016/j.jhazmat.2007.01.132.

Velimirovic M., Auffan M., Carniato L., Mićić Batka V., Schmid D., Wagner S., et al., 2018. Effect of field site hydrogeochemical conditions on the corrosion of milled zerovalent iron particles and their dechlorination efficiency. Science of The Total Environment. 618, 1619-1627. https://doi.org/10.1016/j.scitotenv.2017.10.002.

Vilardi G., Di Palma L., 2017. Kinetic Study of Nitrate Removal from Aqueous Solutions Using Copper-Coated Iron Nanoparticles. Bulletin of Environmental Contamination and Toxicology 98(3), 359-365. https://doi.org/10.1007/s00128-016-1865-9.

Vilardi G., Ochando-Pulido J.M., Verdone N., Stoller M., Di Palma L., 2018. On the removal of hexavalent chromium by olive stones coated by iron-based nanoparticles: Equilibrium study and chromium recovery. Journal of Cleaner Production. 190, 200-210. https://doi.org/10.1016/j.jclepro.2018.04.151.

Vilardi G., Verdone N., Palma L.D., 2017. The influence of nitrate on the reduction of hexavalent chromium by zero-valent iron nanoparticles in polluted wastewater. Desalination & Water Treatment 86, 252-258. https://doi.org/10.5004/dwt.2017.20710.

Vilardi G., Sebastiani D., Miliziano S., Verdone N., Di Palma L., 2018. Heterogeneous nZVI-induced Fenton oxidation process to enhance biodegradability of excavation by-products. Chemical Engineering Journal. 335, 309-320. https://doi.org/10.1016/j.cej.2017.10.152.

Wang W., Hua Y. L. , Li S. L., Yan W. L., Zhang W. X., 2016. Removal of Pb(II) and Zn(II) using lime and nanoscale zero-valent iron (nZVI): A comparative study. Chemical Engineering Journal. 304, 79-88. https://doi.org/10.1016/j.cej.2016.06.069.

Xu G., Ding X., Kuruppu M., Zhou W., Biswas W.. 2018. Research and application of non-traditional chemical stabilizers on bauxite residue (red sand) dust control, a review. Science of The Total Environment. 616, 1552-1565. https://doi.org/10.1016/j.scitotenv.2017.10.158.

Xue W., Huang D., Zeng G., Wan J., Zhang C., Xu R., Cheng M., Deng R., 2018. Nanoscale zero-valent iron coated with rhamnolipid as an effective stabilizer for immobilization of Cd and Pb in river sediments. Journal of Hazardous Materials. 341, 381-389. https://doi.org/10.1016/j.jhazmat.2017.06.028.

Zhang X. W., Kong L. W., Cui X. L., Yin S., 2016. Occurrence characteristics of free iron oxides in soil microstructure: evidence from XRD, SEM and EDS. Bulletin of Engineering Geology and the Environment. 75: 1493-1503. https://doi.org/10.1007/s10064-015-0781-2.

Zong Y. T., Xiao Q., Lu S. G., 2016. Chemical fraction, leachability, and bioaccessibility of heavy metals in contaminated soils, Northeast China. Environmental Science and Pollution Research. 23, 24107-24114. https://doi.org/10.1007/s11356-016-7598-9.
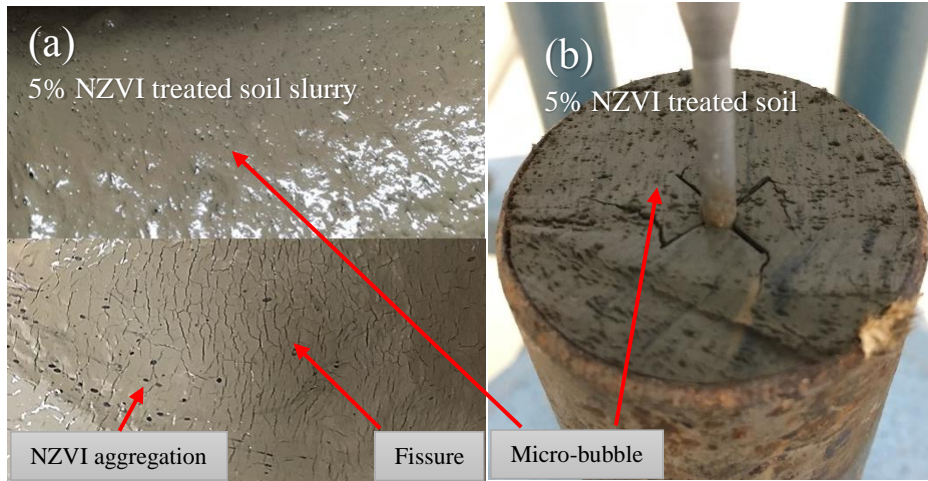
1   Figures List:

2   Figure 1. Flow chart of experimental procedure.

3   Figure 2. Features of soil samples: a) appearance of 5% nZVI treated soil slurry (water content:

4   120%, before the pre-consolidation) and b) laboratory vane shear test of 5% nZVI treated soil

5   sample (after unloading from container).

6   Figure 3. Particle size distribution of the soil samples.

7   Figure 4. Pore size distribution of soil samples determined by MIP in the range from 3 nm to

8   360 μm.

9   Figure 5. X-ray diffraction (XRD) patterns of the soil samples.

10   Figure 6. Sequential relative concentration distribution tendency of Pb in the soil samples (EX,

11   exchangeable fraction, $\times 10$ ng/g; CB, carbonate-bound fraction, $\times 10^3$ ng/g; OX, Fe/Mn oxides-

12   bound fraction, $\times 10^6$ ng/g; OM, organic matter-bound fraction, $\times 10^5$ ng/g; RS, residual fraction,

13    $\times 10^4$ ng/g). Error bars represent relative standard deviations (n = 2).

14   Figure 7. Undrained shear strength results from laboratory vane shear test and moisture content.
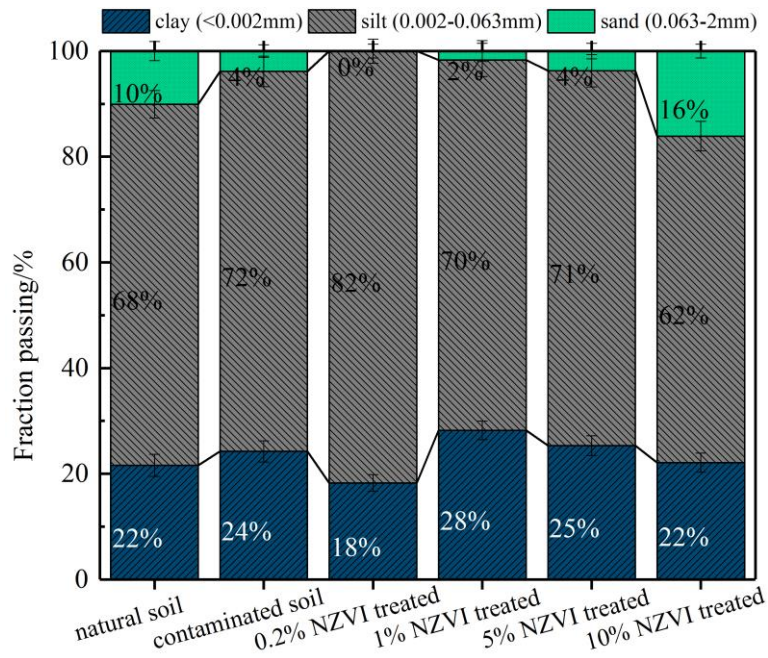
15
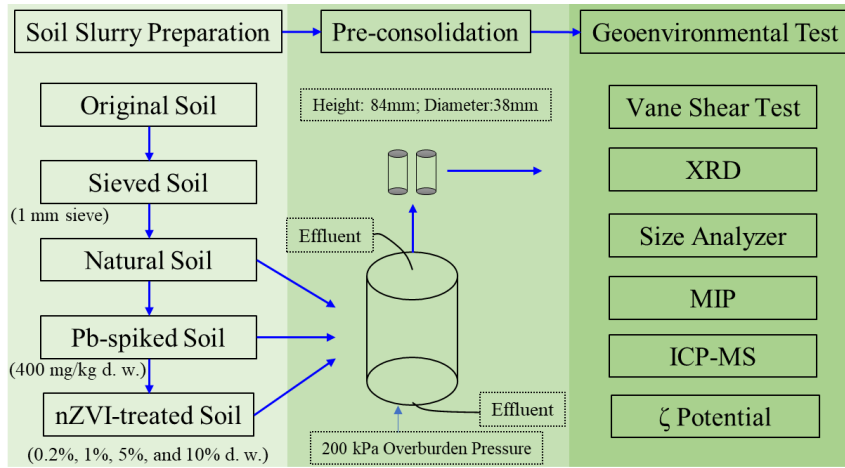
Figure 1. Flow chart of experimental procedure.

1

2

Figure 2. Features of soil samples: a) appearance of 5% nZVI treated soil slurry (water

content: 120%, before the pre-consolidation) and b) laboratory vane shear test of 5% nZVI

treated soil sample (after unloading from container).

1   Figure 3. Particle size distribution of the clayey soil under different treatment conditions.

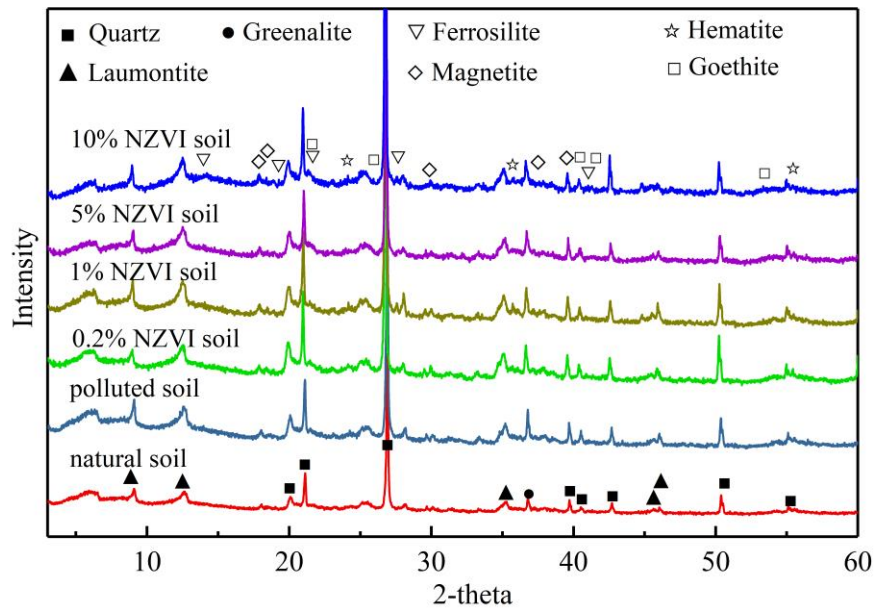2   Error bars represent relative standard deviations (n = 3).

3
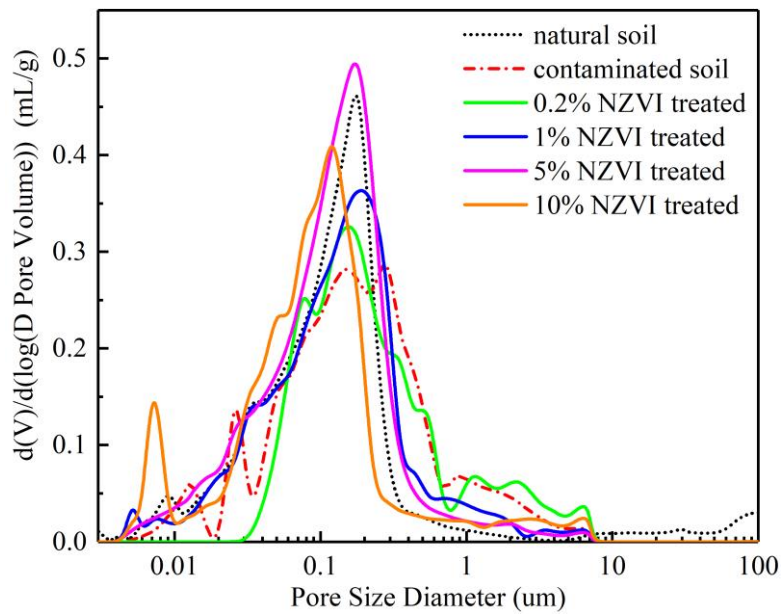
4   Figure 4. Pore size distribution of soil samples determined by MIP in the range 3 nm to 360
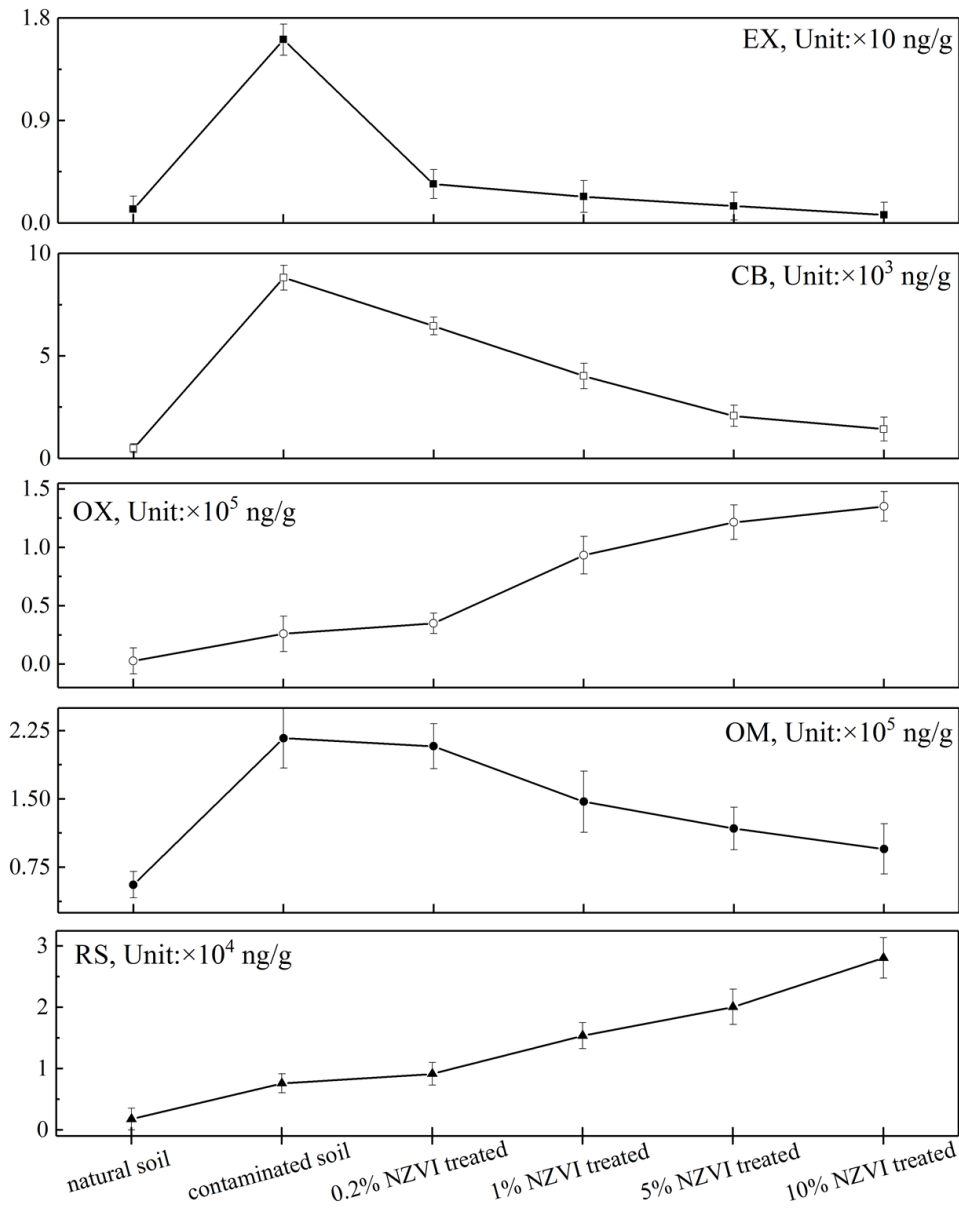
5   μm.

6

Figure 5. X-ray diffraction (XRD) patterns of the soil samples.

1

2

Figure 6. Sequential relative concentration distribution tendency of Pb in the soil samples (EX, exchangeable fraction, ×10 ng/g; CB, carbonate-bound fraction, ×10³ ng/g; OX, Fe/Mn oxides-bound fraction, ×10⁶ ng/g; OM, organic matter-bound fraction, ×10⁵ ng/g; RS, residual fraction, ×10⁴ ng/g) with error bars representing relative standard deviations (n = 2).
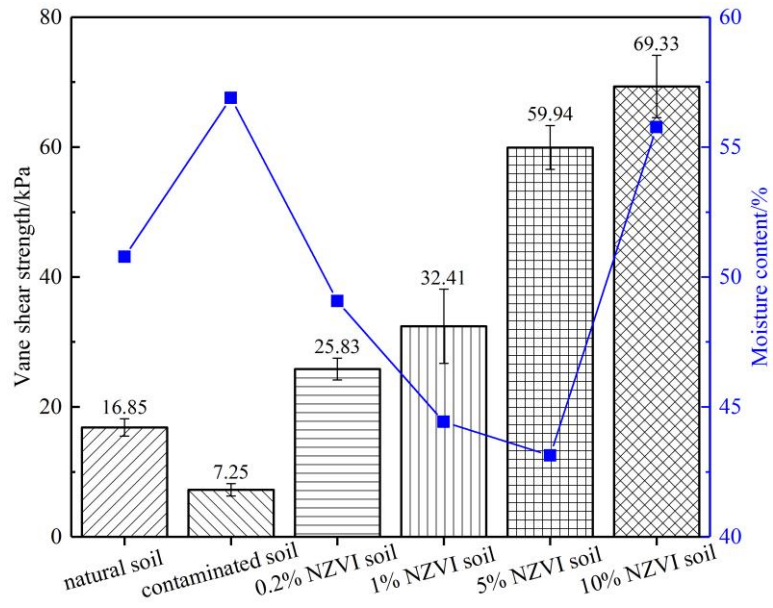
1　　Figure 7. Undrained shear strength results of the laboratory vane shear test versus moisture

2　　　　　　　　　　　　　　　　content.

3

1   Tables list:

2   Table 1. Physicochemical and mechanical properties of clayey soil under different treatment

3   conditions.

4   Table 2. Lattice parameters of the laumontite mineral in soil samples.

5

6

Table 1. Physicochemical and mechanical properties of clayey soil under different treatment conditions.

Item	Natural Soil	Contaminated Soil	0.2% nZVI Treated	1% nZVI Treated	5% nZVI Treated	10% nZVI Treated
Moisture Content /% [a]	50.8	56.9	49.1	44.4	43.1	55.8
Stabilization Efficiency of Pb^{2+} in Exchangeable Fraction/%	-	-	78.8	85.5	90.8	95.6
Stabilization Efficiency of Pb^{2+} in Carbonate-bonding Fraction/%	-	-	26.7	54.4	76.5	83.8
Degree of Saturation (Sr) /%	98.3	95.1	98.9	91.7	94.4	97.2
Vane Shear Strength /kPa	16.9	7.3	25.8	32.4	59.9	69.3
Total Carbon /mg·kg^{-1}	832.1	808.2	797.9	741.5	724.1	705.4
Standard Deviation of TC /mg·kg^{-1}	1.2	1.5	2.0	2.5	1.7	2.2
pH [b]	8.05	8.09	8.34	8.23	8.05	8.00
ζ Potential /mV [c]	-16.14	-6.31	-8.06	-11.60	-8.88	-18.10
Electrical Conductivity / mS/cm [c]	53	46	46	57	95	165
Bulk Density at 0.50 psia /g·cm^{-3} [d]	1.4	1.2	1.0	1.2	1.1	1.2
Apparent (Skeletal) Density /g·cm^{-3} [d]	2.8	1.9	1.4	1.9	2.0	1.9
Porosity /% [d]	49.0	38.4	29.7	38.6	42.7	37.6
Total Pore Area/m^2·g^{-1} [d]	22.7	14.7	6.6	19.0	21.7	27.9
Average Pore Diameter (4V/A) /nm [d]	66.3	90.4	178.4	69.6	69.1	45.7

Note:

[a] refers to the soil samples after unload from the container;

[b] soil pH was measured using a glass electrode in a 1:5 (volume fraction) suspension of soil in water, according to the "international standard specifies an instrumental method for the routine determination of pH" (ISO 10390: 2005);

[c] Zeta potential and electrical conductivity of soil samples was measured at the soil concentration of 1g/L in distilled water;

[d] Soil density and porosity were calculated by Mercury Intrusion Porosimetry (MIP).

1   Table 2. Lattice parameters of the laumontite mineral in soil samples.

Parameter	Natural soil	Contaminated soil	0.2% nZVI treated	1% nZVI treated	5% nZVI treated	10%nZVI treated
a (Å)	15.1902	14.9745	14.8368	14.6733	14.9459	14.8368
b (Å)	13.1902	13.1358	13.16531	13.3037	13.2284	13.1650
c (Å)	7.4170	9.7608	7.5406	7.8429	6.6367	7.5406
β	113.38	106.77	110.37	110.63	113.53	110.37
XS(Å)	429(66)	940(576)	1332(452)	1124(557)	514(178)	311(70)

2   Note: The lattice parameters of laumontite was analyzed using the software of MDI Jade 6.5 and guided

3   by Fridriksson et al. (2003).

4

5

6

7

8

9

10